

---

# A NOVEL PHASE-NOISE MODULE FOR THE QUCS CIRCUIT SIMULATOR. PART II : NOISE ANALYSIS.

---

arXiv PREPRINT

**Torsten Djurhuus** \*  
Goethe-University Frankfurt  
t.djurhuus@physik.uni-frankfurt.de

**Viktor Krozer**  
Goethe-University Frankfurt &  
Ferdinand-Braun-Institut, Leibniz  
Institut für Höchstfrequenztechnik  
krozer@physik.uni-frankfurt.de

March 10, 2026

## ABSTRACT

The paper documents the implementation of a novel phase-noise analysis module within the open-source QUCS circuit simulator environment. The underlying algorithm is based on a rigorous, unified time-domain methodology of (coupled) oscillator noise-response, recently proposed by the authors. The theoretical approach used to develop this model is entirely unconstrained by any empirical and/or phenomenological modelling techniques, such as *e.g.* LTI and LTV theory, and this differentiates it from all prior proposals on this topic. The paper introduces important, and previously unpublished, extensions to this framework, in the form of novel unified closed-form expressions for both the amplitude and phase-amplitude correlation response of a general coupled oscillating circuit perturbed by noise. The proposed theoretic framework translates into highly robust and efficient numerical algorithms, exhibiting several new features and properties which all extend well beyond the scope of the noise analysis tools used in current open-source and/or commercial EDAs. The research discussed herein has many important scientific and industrial applications *w.r.t.* predicting, synthesizing and optimizing the performance of noise-perturbed free-running and coupled autonomous circuits operating under large-signal steady-state conditions. These timing circuits are ubiquitous in all modern communication and remote-sensing systems and the developed simulation tools will prove to have great impact in various areas of industrial circuit design. This paper represents second part of a two-part series with the first part discussing the implementation of the underlying steady-state analysis module. The open-source simulator, discussed and developed herein, applies advanced state-of-the-art stochastic modelling techniques, in-order to produce noise simulation tools with capabilities and scope which, in many areas, exceed what is found in the commercial EDAs currently on the market.

**Keywords** circuits, phase-noise, circuit simulation, noise analysis, oscillators, coupled oscillators, numerical analysis, circuit analysis, autonomous circuits.

## 1 Introduction

Methods for analyzing, synthesizing and optimizing the stochastic response of non-linear circuits, operating under large-signal conditions and perturbed by noise, play a critical role in the design cycle of circuits with important applications in *e.g.* communication and remote-sensing systems. Given the ever-increasing complexity and scale of modern circuit schematics, such work necessitates using an Electronic-Design-Automation (EDA) simulation program.

The work herein considers the development and integration of a novel phase-noise (PNOISE) tool into the Quite Universal Circuit Simulator (QUCS) [1, 2], an open-source distribution published under the GNU General Public License

---

\*The authors are with the Institute of Physics, Goethe University of Frankfurt am Main, Max-von-Laue-Strasse 1, 60438, Frankfurt am Main. (correspondence e-mail: t.djurhuus@physik.uni-frankfurt.de).

(GPL). The resulting extended software package is built as a clone of the QUCS & QUCS-S [3–5] open-source software projects and is referred to as the QUCS-COPEN (working title) distribution/package/project *etc.* In [6], the implementation of the QUCS-COPEN Periodic-Steady-State (PSS) simulator module was covered. The PNOISE tool, discussed herein, depends directly on the numerical output produced by this PSS module. For more details *w.r.t.* these topics<sup>2</sup>, the reader is referred to [6, introduction].

The numerical algorithm behind the QUCS-COPEN PNOISE module, implemented herein, is based on a novel theoretical framework known as the Coupled Oscillator Phase-Macro-Model (COSC-PMM), recently proposed by the authors in [7]. The COSC-PMM framework is constructed using a novel, rigorous and unified time-domain methodology which involves techniques and ideas spanning various branches of mathematics, including differential geometry, topology, Floquet theory and nonlinear stochastic integration. It represents a direct extension of the established, and highly cited, single/free-running oscillator Phase Macro Model (PMM) [8–10]. As was documented in [7], the COSC-PMM includes the single oscillator PMM as a special case, and hence not only extends but also replaces this previously published model. The novel COSC-PMM framework represents the only ever published Linear-Response (LR) model description of coupled oscillator noise-response which does not rely on some form of empirical and/or phenomenological modelling approach, such as *e.g.* linear-time-invariant (LTI), linear-time-variant (LTV) theory, block-diagram models *etc.* All previously proposed models, ever published on this topic, can hence correctly, and without hyperbole, be characterized as incomplete. A prominent example hereof is the Conversion-Matrix (C-MATRIX) methodology where the response is calculated using noise-folding/mixing techniques. This frequency-domain description models the large-signal oscillating circuit as an internally driven nonlinear mixer with the noise signals being fed into the linear RF port. By definition, this represents a LTV approach. The C-MATRIX LTV methodology has long been favored by a majority of researches in the scientific community as a direct approach for developing robust numerical algorithms. As a result, most established commercial EDAs, such as *e.g.* Keysight-ADS<sup>®</sup> and Cadence SpectreRF<sup>®</sup>, all apply this methodology in their implementation of large-signal noise analysis tools. Despite such proven use-cases it is, nevertheless, a well-established fact [8, 9, 11] that these LTV C-MATRIX models, applied to (coupled) oscillating systems perturbed by noise, are unable to fully capture the underlying stochastic response; a fact which manifests in an artificial singularity at the carrier (zero offset) in the calculated spectrum [8, 9, 11]. As this singularity is approached, numerical noise will accumulate in the calculated solution rendering the output of the algorithm dubious and unreliable. As such, this issue not only invalidates the calculated spectrum directly at the singularity, but also corrupts the solution in some open range of this point [11]. These types of fundamental and structural problems remain an inescapable reality when dealing with any empirical or phenomenological model as the underlying theoretic description, by definition, must be incomplete and lacking.

As the only complete, non-phenomenological/empirical LR model of coupled oscillator noise-response, the COSC-PMM is not tainted by any of the problems or issues described above. The produced spectrum is correctly calculated at all offsets from the carrier, no artificial singularities are observed in the output and no numerical noise issues invalidates the computed result or plays any role in the performance of the method. The QUCS-COPEN package is the first ever, to our knowledge, EDA project to include a PNOISE module based on the novel COSC-PMM methodology. Consequently, it is thus also the first ever EDA project to include a PNOISE analysis module, applicable to coupled circuits, which is correct, in the strictest sense, meaning that it does not rely on any kind of LTV, LTI, block-diagram or other phenomenological/empirical modelling approach to calculate the spectrum.

### 1.1 A Note on Alternative Open-Source Engines : qucsatorRF, GnuCap, ngspice & Xyce.

The QUCS-S [3–5] software package ships with its own qucsator engine clone called qucsatorRF (see footnote 2) and both the QUCS [1, 2] and QUCS-S packages link to other non-QUCS, SPICE based, open-source simulator engines, including : GnuCap [12], ngspice [13] and Xyce [14]. All these external engines were discussed in [6] and the reader should consult this paper for details. From [6], only the ngspice packages supported any type of PSS analysis of autonomous simulation. Likewise, the ngspice manual also contains the only mention of large-signal noise analysis of autonomous circuits. Quoting the ngspice manual [13, sec. 1.2.8] : "Results of PSS are the basis of periodical large-signal analysis like PAC or PNoise". As was the case with the ngspice PSS module this noise analysis implementation is labelled *experimental code* (see discussion in [6]). Furthermore, neither the PAC or PNoise modules, as far as we can tell, are mentioned anywhere else in the ~750 page manual. Given these facts, one must conclude that these features have not yet been implemented or, at the very least, have not yet been properly tested or documented. Thus, a review of the current state of the available open-source simulator engines, *w.r.t.* available PNOISE tools, leads to only one conclusion : no credible alternative options exist for analysis of large-signal noise-response of autonomous circuits (clocks/oscillators), not to mention coupled circuits, in any of the major open-source simulator engines discussed here.

<sup>2</sup>A very brief recap (for completeness) : the new QUCS-COPEN package is constructed from an extended version of the QUCS simulator engine, called qucsator, which is then linked with a Graphical-User-Interface (GUI) schematic capture application taken from the QUCS-S distribution and modified to suit the needs of the new QUCS-COPEN simulator.

## 1.2 Outline of paper

Below, various theoretical and practical aspects *w.r.t.* the COSC-PMM methodology and the implementation of the QUCS-COPEN PNOISE analysis tool, are discussed. Sections 2, 2.1 and 2.2 reviews the theory behind the COSC-PMM framework and the corresponding implemented numerical algorithm. In Section 2.3 the original COSC-PMM scheme, proposed in [7], which was limited to the phase-noise response, is extended to include expressions for both the amplitude and cross-correlation noise response components. These important additions are published herein for the first time and will serve to further improve the scope of the COSC-PMM model framework. Sections 2.4 and 2.5 cover the various practical issues involved *w.r.t.* the actual implementation & integration of the PNOISE tool into the QUCS-COPEN package<sup>3</sup>. In section 3, the newly implemented QUCS-COPEN noise analysis module will be demonstrated on a varied set of example oscillator circuits, both coupled and free-running. Then in section 3.2, the calculated results are validated through a comparison study with the commercial Keysight-ADS<sup>®</sup> simulator. Finally, section 4 summarizes the obtained results and outlines future work & projects, currently in the pipeline *w.r.t.* to the QUCS-COPEN project.

## 2 Background Theory & PNOISE Module Implementation.

The noise-perturbed circuit equations (KCL/KVL) are written using a standard Modified-Nodal-Analysis (MNA) notation [16]<sup>4</sup>

$$\dot{q}(x(t)) + i(x(t)) + s(t) + B(x(t))\xi(t) = 0 \quad (1)$$

where,  $x(t) : \mathbb{R} \rightarrow \mathbb{R}^n$ , represents the  $n$ -dimensional circuit state, vectors  $q(x), i(x) : \mathbb{R}^n \rightarrow \mathbb{R}^n$ , hold the reactive and resistive (KCL/KVL) contributions, respectively,  $s(t) : \mathbb{R} \rightarrow \mathbb{R}^n$  contain the contributions of all independent sources in the circuit,  $B(\cdot) : \mathbb{R}^n \rightarrow \mathbb{R}^{n \times p}$  is the *noise modulation matrix* [8–10] and  $\xi(t) : \mathbb{R} \rightarrow \mathbb{R}^p$  holds  $p$  uncorrelated, zero-mean, unit-power white-noise sources.

The topic of discussion here is noise-analysis of autonomous circuits operating under large-signal conditions, which implies the existence of a special asymptotic periodic solution to (noise-free) eq. (1),  $x_s(t) : \mathbb{R} \rightarrow \mathbb{R}^n$ , the so-called Periodic Steady State (PSS). This solution is assumed stable and periodic,  $x_s(t_0 + T_0) - x_s(t_0) = 0$ , where  $t_0, T_0 \in \mathbb{R}_+$  are parameters representing some asymptotic time offset and the steady-state period, respectively. The limit-cycle,  $\gamma$ , represents the unique 1-dimensional  $\omega$ -limit set (attractor) traced out by the asymptotic PSS solution. Thus,  $x_s(\eta) \in \gamma$ , for all  $\eta$  and,  $\lim_{t \rightarrow \infty} \|x(t) - \gamma\| = 0$ , for any solution  $x(t)$  to eq. (1) inside the stable manifold (*i.e.* the basin of attraction) of  $\gamma$ . The paper [6] (part-I of series) contains a review of the various proposed methods for deriving this solution numerically, including a detailed description of the specific methodology used to implement the QUCS-COPEN PSS analysis module.

### 2.1 Deriving the Floquet Decomposition.

Given the PSS,  $x_s(t) : \mathbb{R} \rightarrow \mathbb{R}^n$ , (see [6] for details), the circuit equations in eq. (1) can be linearized around this solution. The resulting MNA Linear-Response (LR) equations have the form

$$d(C(t)\delta x(t))/dt + G(t)\delta x(t) = 0 \quad (2)$$

where,  $\delta x(t) : \mathbb{R} \rightarrow \mathbb{R}^n$ , is the LR state vector and  $C(t)=dq(s)/ds, G(t)=di(s)/ds|_{s=x_s(t)} : \mathbb{R} \rightarrow \mathbb{R}^{n \times n}$ , are two time-dependent, periodic Jacobian matrices governing the linearized dynamics, with  $i, q$  defined above in eq. (1). The PSS is assumed stable and a solution to eq. (2) is then calculated by integrating these differential equations forward in time. As the system in eq. (2) is linear this solution can be expressed in-terms of the system State-Transition-Matrix (STM)  $\Phi(t, s) : \mathbb{R} \times \mathbb{R} \rightarrow \mathbb{R}^{n \times n}$ . Furthermore, with the time-dependence being periodic, this STM can be decomposed using Floquet theory [16]

$$\Phi(t, s) = \sum_{i=1}^n u_i(t) \exp(\mu_i[t - s]) v_i^\top(s) C(s) \quad (3)$$

<sup>3</sup>The text in sections 2.4 and 2.5 will, in places, contain brief discussion of C++ code [15] (the QUCS program language) including the use of some C++ notation and keywords.

<sup>4</sup>The noise-free version of eq. (1) was analyzed in part-I [6] of this series. Hence, brief passages of text in this section, involving steady-state (*i.e.* noise-free, PSS) topics, may constitute a repeat (to some degree) of the discussion in [6]. This approach was chosen in the interest of completion and readability.

where  $\mu_i \in \mathbb{C}$  is the  $i$ th Floquet characteristic exponent,  $u_i(t), v_i(t) : \mathbb{R} \rightarrow \mathbb{C}^n$  are the  $i$ th,  $T_0$  periodic, Floquet and dual Floquet vectors, respectively, and the  $T_0$  periodic Jacobian matrix,  $C(t) : \mathbb{R} \rightarrow \mathbb{R}^{n \times n}$ , was defined above in eq. (2). From eq. (3), the Monodromy Matrix (MM),  $\Phi_M \in \mathbb{R}^{n \times n}$ , is derived as

$$\Phi_M \equiv \Phi(T_0, 0) = \sum_{i=1}^n \lambda_i u_i(T_0) v_i^\top(0) C(0) \quad (4)$$

where  $\lambda_i = \exp(\mu_i T_0)$  is the  $i$ th Floquet characteristic multiplier. Given periodicity,  $u_i(0) = u_i(T_0)$ , and the orthogonality condition,  $v_i^\top(t) C(t) u_j(t) = \delta_{ij}$  [16], it follows from inspection of eq. (4) that  $u_i(0)$  is an eigenvector of the MM with eigenvalue  $\lambda_i$ , and in this way, the entire set,  $\{u_i(0)\}_{i=1}^n$ , is derived. Using this set of eigenvectors as initial conditions, the system in eq. (2) is integrated forward in time to produce the complete set of time-periodic Floquet vectors  $\{u_i(t)\}_{i=1}^n$  [8, 9, 17]. This set spans the so-called tangent-bundle<sup>5</sup> along the limit-cycle base-space [7, 17]

$$\mathbb{T}_\gamma \mathbb{M} = \text{span}\{u_1(t), u_2(t), \dots, u_n(t)\} \quad (5)$$

The adjoint LR equations, corresponding to the system in eq. (1), are written [16]

$$C^\top(t) d(\delta x(t))/dt - G^\top(t) \delta x(t) = 0 \quad (6)$$

A solution to eq. (6), for a given initial condition, can be found by integrating this system backwards in time. This solution is then expressed in-terms of the adjoint STM

$$\Psi(t, s) = \sum_{i=1}^n v_i(t) \exp(-\mu_i [t - s]) u_i^\top(s) C^\top(s) \quad (7)$$

and the corresponding adjoint MM is given as

$$\Psi_M \equiv \Psi(-T_0, 0) = \sum_{i=1}^n \lambda_i v_i(-T_0) u_i^\top(0) C^\top(0) \quad (8)$$

Repeating the arguments introduced above,  $v_i(0)$  is an eigenvector of the adjoint MM in eq. (8) with eigenvalue  $\lambda_i$  and the dual set,  $\{v_i(t)\}_{i=1}^n$ , is calculated by integrating eq. (6), with this initial eigenvector-set, backwards in time. The dual Floquet vectors span the dual tangent bundle (see footnote 5) along the limit-cycle base-space

$$\mathbb{T}_\gamma^* \mathbb{M} = \text{span}\{v_1(t), v_2(t), \dots, v_n(t)\} \quad (9)$$

### 2.1.1 The Concept of a Floquet Mode & Floquet Mode Response.

Herein the Floquet vector function,  $u_i(t)$ , is often referred to as the  $i$ th Floquet mode. Sometimes, the entire triplet of operators  $\{u_i(t), v_i(t), \mu_i\}$  is also referred to as such. The  $i$ th Floquet mode response,  $z_i(t) : \mathbb{R} \rightarrow \mathbb{C}^n$ , then represents the projected noise-driven LR dynamics along the  $i$ th Floquet mode,  $z_i(t) = \kappa_i(t) u_i(t)$ , where  $\kappa_i : \mathbb{R} \rightarrow \mathbb{C}$  is the first-order noise-response along this vector. From eqs. (1) and (3) it follows that

$$\kappa_i(t) = \int_{-\infty}^t \exp(\mu_i [\eta - t]) v_i^\top(\eta) C(\eta) B(x_s(\eta)) \xi(\eta) d\eta \quad (10)$$

with noise operators,  $B, \xi$ , defined in eq. (1). Importantly, we will often also refer to the mode response,  $z_i(t)$ , as the  $i$ th mode for simplicity. This should not cause any confusion.

<sup>5</sup>A tangent-space,  $\mathbb{T}_x \mathbb{M}$ , on a  $k$ -dimensional sub-manifold,  $\mathbb{M}$ , of  $\mathbb{R}^n$ , at the point  $x$ , is an affine copy of vector-space  $\mathbb{R}^k$  with origin at  $x$ . A tangent-bundle along an embedded set,  $\gamma \in \mathbb{M}$ , then simply refers to the disjoint union of these tangent-spaces along this base-space *i.e.*  $\mathbb{T}_\gamma \mathbb{M} = \cup_{x \in \gamma} \mathbb{T}_x \mathbb{M}$ . This description also holds for the special case  $\mathbb{M} = \mathbb{R}^n$  (*i.e.* no sub-manifold) Likewise, a dual (co-variant) tangent-space,  $\mathbb{T}_x^* \mathbb{M}$ , on the  $k$ -dimensional sub-manifold,  $\mathbb{M}$ , of  $\mathbb{R}^n$ , at the point  $x$ , is an affine copy of dual vector-space  $\mathbb{R}^{k*}$  with origin at  $x$ . Equivalently, a dual tangent-bundle is defined as  $\mathbb{T}_\gamma^* \mathbb{M} = \cup_{x \in \gamma} \mathbb{T}_x^* \mathbb{M}$  which again also holds for the special case  $\mathbb{M} = \mathbb{R}^n$ .

### 2.1.2 The Special PSS Floquet Mode.

It is a well-established fact [8–10, 17] that autonomous circuits, with a stable PSS, will produce a special single real Floquet mode with zero characteristic exponent. This special operator, traditionally represented by the first mode  $\{u_1, v_1, \mu_1 = 0\}$ , is special and unique as it is the only mode, assuming an asymptotically stable PSS, that has a Floquet characteristic exponent equal to zero  $\mu_1 = 0 \Rightarrow \lambda_1 = 1$ . It describes the LR dynamics projected onto the tangent-direction of the limit-cycle,  $\gamma$ , with  $u_1(t) \propto \dot{x}_s(t)$  for all  $t$ . The dynamics in this direction are neutrally stable, *i.e.* no retracting force, which is characterized mathematically by a characteristic exponent with real part equal to zero. Let,  $\alpha(t) : \mathbb{R} \rightarrow \mathbb{R}$ , describe the phase offset along  $\gamma$  caused by the noise perturbations projected onto this set. From eq. (10), one can derive an expression for the phase increment

$$\alpha(t + \tau) - \alpha(t) = \int_t^{t+\tau} v_i^\top(\eta) C(\eta) B(x_s(\eta)) \xi(\eta) d\eta \quad (11)$$

The increment in eq. (11) is bounded, however, it should be clear that the phase variable,  $\alpha(t)$ , itself is not. In fact, it is a well established result [8–10, 17] that, asymptotically with time, this variable becomes normally distributed with power  $\langle (\alpha(t) - \kappa)^2 \rangle = ct$  where the positive scalar,  $c \in \mathbb{R}_+$ , is known as the *phase diffusion constant*, and  $\kappa$  represents the asymptotic mean value.

## 2.2 The Novel COSC-PMM Modelling Framework.

The model considers  $k$  free-running, asymptotically stable autonomous oscillator units coupled through some type of network. This circuit topology is referred to as a  $k$ -ensemble. It is assumed that the ensemble reaches a  $T_0 \in \mathbb{R}_+$  periodic synchronized state,  $x_s(t_0) = x_s(t_0 + T_0)$ , *i.e.* the ensemble PSS. The concept of a unique *phase-manifold*,  $\mathcal{M}$ , corresponding to a given  $k$ -ensemble configuration, was first discussed in the paper [7], recently published by the authors. It refers to a closed,  $k$ -dimensional, smooth sub-manifold embedded in  $n$ -dimensional state-space,  $\mathbb{R}^n$ , and parameterized by a set of coordinates indexing the phase-state of the coupled circuit. Using various established results and ideas from topology and differential geometry, the existence of this unique manifold was proven for a synchronized circuit in [7]. The analysis further showed how the ensemble limit-cycle,  $\gamma$ , constitutes a 1-dimensional sub-manifold embedded in this space, *i.e.*  $\gamma \hookrightarrow \mathcal{M}$ . Let  $\mathbb{T}_\gamma \mathcal{M}$  represent the tangent-bundle (see eq. (5) and footnote 5) along  $\gamma$  on  $\mathcal{M}$ . A standard result of COSC-PMM theory, introduced in [7], then predicts the existence of exactly  $k$  unique Floquet modes spanning this bundle. As the numbering of Floquet modes is arbitrary we are free to choose these to be the first  $k$  vectors in the set

$$\mathbb{T}_\gamma \mathcal{M} = \text{span}\{u_1(t), u_2(t), \dots, u_k(t)\} \quad (12)$$

with the remaining set of  $n-k$  Floquet vectors spanning the amplitude bundle  $\mathbb{T}_\gamma \mathcal{J}$  [7]. From eq. (5), the tangent-bundle along  $\gamma$  is then decomposed into phase and amplitude sub-bundles as

$$\mathbb{T}_\gamma \mathbb{R} = \mathbb{T}_\gamma \mathcal{M} \oplus \mathbb{T}_\gamma \mathcal{J} \quad (13)$$

Let  $\{\phi_i(t)\}_{i=1}^k$  denote the  $k$  Floquet modes<sup>6</sup> on  $\mathbb{T}_\gamma \mathcal{M}$ , which govern the LR noise-driven phase dynamics on  $\mathcal{M}$ ; *i.e.* the *phase-modes*. Likewise,  $\{\psi_i(t)\}_{i=1}^{n-k}$  then refers to the set of  $n-k$  *amplitude-modes* (see footnote 6) governing the LR noise amplitude dynamics in directions not tangential to  $\mathcal{M}$ . Referring to section 2.1.2, the first phase-mode  $\{u_1, v_1, \mu_1 = 0\}$ , requires special attention. As the response,  $\alpha(t) : \mathbb{R} \rightarrow \mathbb{R}$  grows without bound this response cannot be linearized and must be included in the total phase of the various operators. For this purpose the effective time-variable  $\iota(t) : \mathbb{R} \rightarrow \mathbb{R}$  is introduced

$$\iota(t) = t + \alpha(t) \quad (14)$$

The remaining response is collected in the residual phase and amplitude actions  $\Phi_\delta, \Psi_\delta : \mathbb{R} \rightarrow \mathbb{R}^n$ ,

$$\Phi_\delta(\iota(t)) = \sum_{i=2}^k \phi_i(\iota(t)), \quad A_\delta(\iota(t)) = \sum_{i=1}^{n-k} \psi_i(\iota(t)) \quad (15)$$

<sup>6</sup>Note, that strictly speaking, operators  $\phi_i(t)$  &  $\psi_i(t)$  represent *mode responses* characterizing noise driven phase/amplitude LR along the  $i$ th phase/amplitude Floquet mode (*i.e.* corresponding Floquet vectors, see section 2.1.1). However, as explained in section 2.1.1, for simplicity, these operators will also be referred to herein as *modes*.

where the residual phase LR action is seen to exclude the special first mode (sum index starts at  $i = 2$ ) for the exact reasons mentioned in section 2.1.2 and above in connection with eq. (14). Given this setup, an expression for the  $k$ -ensemble LR, on the phase-manifold  $\mathcal{M}$ , and tangential to this space, can be written as

$$x_{\text{LR}}(t)|_{\mathcal{M}, \text{tangential}} = x_{\text{LR}}(t)|_{\mathbb{T}, \gamma} = x_s(\iota(t)) + \Phi_\delta(\iota(t)) \quad (16)$$

Since the above relation is restricted to direction tangential  $\mathcal{M}$ , it describes the *phase-noise response* of the coupled circuit. From eq. (16), an expression for the asymptotic system correlation matrix on  $\mathcal{M}$ ,  $C_s(\tau) : \mathbb{R} \rightarrow \mathbb{C}^{n \times n}$ , can be produced. The corresponding power spectral density,  $\mathfrak{L}^{(\nu)} : \mathbb{R} \rightarrow \mathbb{R}$ , *i.e.* the PNOISE spectrum, around the  $\nu$ th harmonic of the PSS carrier, then follows from Fourier transforming the  $\nu$ th harmonic envelope of  $C_s(\tau)$ . The procedure described here was carried out in [7, sec. 6] and following some rather lengthy and involved calculations, the following expression, slightly re-written, was derived

$$\mathfrak{L}^{(\nu)}(\omega_m^{(\nu)}) = \frac{(1 - a^{(\nu)})(\omega_0^2 \nu^2 c) - 2b^{(\nu)}\omega_m}{(0.5\omega_0^2 \nu^2 c)^2 + (\omega_m^{(\nu)})^2} + \sum_{\rho} \sum_{l=1}^{k-1} \frac{\Upsilon_{l\rho}^{(\nu)} [2|\mu_{l+1,r}| + (\omega_0^2 \rho^2 c)] + 2\Delta_{l\rho}^{(\nu)} [\omega_m^{(\nu)} + \mu_{l+1,i}]}{(|\mu_{l+1,r}| + (0.5\omega_0^2 \rho^2 c))^2 + (\omega_m^{(\nu)} + \mu_{l+1,i})^2} \quad (17)$$

with  $\omega_0 = 2\pi/T_0$  being the operating frequency of the synchronized ensemble,  $\mu_s = \mu_{s,r} + j\mu_{s,i} \in \mathbb{C}$ , is the  $s$ th characteristic Floquet exponent (real/imaginary parts) and  $\omega_m^{(\nu)} = \omega - \nu\omega_0$  is the  $\nu$ th harmonic offset frequency. The real parameter,  $c \in \mathbb{R}_+$ , is known as the *phase-diffusion* constant [8, 10, 17] (see also section 2.1.2). All summations in eq. (17) without bounds operate in the interval  $(-\infty, \infty)$ . The operators  $a^{(\nu)}, b^{(\nu)}, \Upsilon_{l\rho}^{(\nu)}, \Delta_{l\rho}^{(\nu)}$  introduced in eq. (17) are defined through<sup>7</sup>  $a^{(\nu)} + jb^{(\nu)} = \overline{q\Omega^{(\nu)}}$  and  $\Upsilon_{l\rho}^{(\nu)} + j\Delta_{l\rho}^{(\nu)} = \overline{q\Theta_{l\rho}^{(\nu)}}$ , where index  $q$  refers to the index of the *observation-node* *i.e.* the node where PNOISE is measured (see footnote 7). The two complex tensor operators  $\Omega$  and  $\Theta_{l\rho} \in \mathbb{C}^{n \times n}$ , used in the above definitions, have the form (see [7, appendix D] for details)

$$\Omega^{(\nu)} = \sum_{m=2}^k \sum_p \frac{U_{1,\nu} \Lambda_{1,0}^\top \Lambda_{m,\nu-p}^* U_{m,p}^\dagger}{j\omega_0(p-\nu) - \mu_m^*} \quad (18)$$

$$\Theta_{l\rho}^{(\nu)} = \frac{U_{1,\rho} \Lambda_{1,0}^\top \Lambda_{l+1,\rho-\nu}^* U_{l+1,\nu}^\dagger}{j\omega_0(\nu-\rho) - \mu_{l+1}^* - \mu_1} + \sum_{i=2}^k \sum_p \frac{U_{i,p} \Lambda_{i,\rho-p}^\top \Lambda_{l+1,\rho-\nu}^* U_{l+1,\nu}^\dagger}{j\omega_0(\nu-p) - \mu_{l+1}^* - \mu_i} \quad (19)$$

where  $U_{i,j} \in \mathbb{C}^n$  is the  $j$ th harmonic of the  $i$ th Floquet vector  $u_i(t) : \mathbb{R} \rightarrow \mathbb{C}^n$  and  $\Lambda_{i,j} \in \mathbb{C}^n$  is the  $j$ th harmonic of the  $i$ th Floquet lambda-vector,  $\lambda_i(t) : \mathbb{R} \rightarrow \mathbb{C}^n$ , where  $\lambda_i(t) = v_i^\top(t)B(x_s(t))$ , with  $v_i(t) : \mathbb{R} \rightarrow \mathbb{C}^n$  being the  $i$ th Floquet phase-mode dual-vector (see section 2.1). Finally,  $B(x_s(t)) : \mathbb{R} \rightarrow \mathbb{R}^{n \times p}$  is the noise modulation matrix, see [7–10] and eq. (1), which describes how  $p$  unit-power, zero-mean white-noise sources are injected into the  $n$ -dimensional state-space, the power of these sources and the manner in which the sources are modulated by the PSS.

### 2.3 Expanding the COSC-PMM Framework : Adding Amplitude and Correlation Contributions.

Using the definition of residual phase and amplitude response in eq. (15) the complete LR state-vector is written

$$x_{\text{LR}}(t)|_{\mathcal{M}} = x_s(\iota(t)) + \Phi_\delta(\iota(t)) + A_\delta(\iota(t)) \quad (20)$$

From eq. (20), the system correlation matrix,  $C_s(\tau) = \lim_{t \rightarrow \infty} \langle x_{\text{LR}}(t)x_{\text{LR}}^\dagger(t+\tau) \rangle$ , is decomposed as follows

$$C_s(\tau) = C_{\Phi\Phi}(\tau) + C_{\Phi A}(\tau) + C_{AA}(\tau) \quad (21)$$

where,  $C_{\Phi\Phi}, C_{\Phi A}, C_{AA} : \mathbb{R} \rightarrow \mathbb{R}^{n \times n}$ , represent the COSC-PMM asymptotic phase, cross-correlation and amplitude correlation matrices for the synchronized  $k$ -ensemble, respectively, with

<sup>7</sup>Let  $M^{(\nu)} \in \mathbb{C}^{n \times n}$  be some square, complex matrix (within the COSC-PMM methodology) with superscript  $\nu$  referring to the PSS harmonic index discussed in connection with eq. (17). Then let,  ${}_q M^{(\nu)} = [M^{(\nu)}]_{q,q} / \|X_{s,\nu}^{[q]}\|^2$ , where  $[Q]_{i,j}$  denotes to the element at row  $i$  and column  $j$  of matrix  $Q$  and  $X_{s,\nu}^{[q]}$  refers to the  $q$ th element of the PSS  $\nu$ th harmonic vector. Hence,  ${}_q M^{(\nu)}$  is the  $q$ th diagonal matrix element, normalized by the  $\nu$ th harmonic power, of the  $q$ th PSS vector component.

$$C_{\Phi\Phi}(\tau) = \lim_{t \rightarrow \infty} \langle [x_s(\iota(t)) + \Phi_\delta(\iota(t))] [x_s(\iota(t + \tau)) + \Phi_\delta(\iota(t + \tau))]^\dagger \rangle \quad (22)$$

$$C_{\Phi A}(\tau) = \lim_{t \rightarrow \infty} \langle x_s(\iota(t)) A_\delta^\dagger(\iota(t + \tau)) \rangle + \lim_{t \rightarrow \infty} \langle \Phi_\delta(\iota(t)) A_\delta^\dagger(\iota(t + \tau)) \rangle + \langle \dots \rangle^\dagger \quad (23)$$

$$C_{AA}(\tau) = \lim_{t \rightarrow \infty} \langle A_\delta(\iota(t)) A_\delta^\dagger(\iota(t + \tau)) \rangle \quad (24)$$

Fourier transforming the  $q$ th diagonal component, of the  $\nu$ th harmonic envelope, of eq. (22) produces an expression for the  $k$ -ensemble phase-noise spectrum, around the  $\nu$  harmonic and for the  $q$ th measurement node, which was done in [7] and with this result repeated in eqs. (17) to (19). Similarly, components of the correlation matrices in eqs. (23) and (24) can be transformed to produce the cross-correlation and amplitude spectra,  $\mathcal{R}^{(\nu)}, \mathcal{A}^{(\nu)} : \mathbb{R} \rightarrow \mathbb{R}$ .

### 2.3.1 The COSC-PMM Amplitude Noise Spectrum.

Inspecting eqs. (15) and (24), it follows that calculating the asymptotic amplitude correlation matrix,  $C_{AA}(\tau) : \mathbb{R} \rightarrow \mathbb{C}^{n \times n}$ , involves evaluating terms of the type  $\langle \psi_i(t) \psi_j(t + \tau) \rangle$ , where,  $\psi_i : \mathbb{R} \rightarrow \mathbb{C}^n$ , is the  $i$ th amplitude Floquet mode as defined above in connection with eq. (15) (see also section 2.1.1 and footnote 6). The techniques used for calculating this type of ensemble average was thoroughly covered in [7]. Following the procedure laid out in appendix B of [7] an expression for the amplitude spectrum  $\mathcal{A}^{(\nu)} : \mathbb{R} \rightarrow \mathbb{R}$ , can be derived

$$\mathcal{A}^{(\nu)}(\omega_m^{(\nu)}) = \sum_{\rho} \sum_{l=1}^{n-k} \frac{W_{l\rho}^{(\nu)} [2|\mu_{l+k,r}| + (\omega_0^2 \rho^2 c)] + 2T_{l\rho}^{(\nu)} [\omega_m^{(\nu)} + \mu_{l+k,i}]}{(|\mu_{l+k,r}| + (0.5\omega_0^2 \rho^2 c))^2 + (\omega_m^{(\nu)} + \mu_{l+k,i})^2} \quad (25)$$

where  $W_{l\rho}^{(\nu)} + jT_{l\rho}^{(\nu)} = \overline{q\Pi_{l\rho}^{(\nu)}}$  (see footnote 7) and

$$\Pi_{l\rho}^{(\nu)} = \sum_{i=k+1}^n \sum_p \frac{U_{i,p} \Lambda_{i,\rho-p}^\top \Lambda_{l+k,\rho-\nu}^* U_{l+k,\nu}^\dagger}{j\omega_0(\nu-p) - \mu_{l+k}^* - \mu_i} \quad (26)$$

### 2.3.2 The COSC-PMM Cross-Correlation Noise Spectrum

The amplitude-phase cross-correlation matrix is written in eq. (23) with the various operators defined in eqs. (15) and (20). It involves calculating terms of the type  $\langle x_s(t + \alpha(t)) \psi_j^\dagger(t + \tau) \rangle$  and  $\langle \psi_i(t) \phi_j^\dagger(t + \tau) \rangle$  where  $\phi_i, \psi_i$  represent the  $i$ th residual phase and amplitude Floquet modes, respectively. Again, following the procedure laid out in appendix B of [7], which explains how to calculate both of these two types ensemble averages, an expression for the cross-correlation spectrum  $\mathcal{R}^{(\nu)} : \mathbb{R} \rightarrow \mathbb{R}$ , can be derived

$$\mathcal{R}^{(\nu)}(\omega_m^{(\nu)}) = -\frac{t^{(\nu)}(\omega_0^2 \nu^2 c) + 2u^{(\nu)}\omega_m}{(0.5\omega_0^2 \nu^2 c)^2 + (\omega_m^{(\nu)})^2} + \sum_{\rho} \sum_{l=1}^{n-1} \frac{E_{l\rho}^{(\nu)} [2|\mu_{l+1,r}| + (\omega_0^2 \rho^2 c)] + 2Z_{l\rho}^{(\nu)} [\omega_m^{(\nu)} + \mu_{l+1,i}]}{(|\mu_{l+1,r}| + (0.5\omega_0^2 \rho^2 c))^2 + (\omega_m^{(\nu)} + \mu_{l+1,i})^2} \quad (27)$$

where,  $t^{(\nu)} + ju^{(\nu)} = q\overline{\Psi^{(\nu)}}$ ,  $E_{l\rho}^{(\nu)} + jZ_{l\rho}^{(\nu)} = q\overline{\Xi_{l\rho}^{(\nu)}}$  (see footnote 7) and

$$\Psi^{(\nu)} = \sum_{m=k+1}^n \sum_p \frac{U_{1,\nu} \Lambda_{1,0}^\top \Lambda_{m,\nu-p}^* U_{m,p}^\dagger}{j\omega_0(p-\nu) - \mu_m^*} \quad (28)$$

$$\Xi_{l\rho}^{(\nu)} = \begin{cases} \sum_{i=k+1}^n \sum_p \frac{U_{i,p} \Lambda_{i,\rho-p}^\top \Lambda_{l+1,\rho-\nu}^* U_{l+1,\nu}^\dagger}{j\omega_0(\nu-p) - \mu_{l+1}^* - \mu_i} & \text{for } l \leq k-1 \\ U_{1,\rho} \Lambda_{1,0}^\top \Lambda_{l+1,\rho-\nu}^* U_{l+1,\nu}^\dagger + \sum_{i=2}^k \sum_p \frac{U_{i,p} \Lambda_{i,\rho-p}^\top \Lambda_{l+1,\rho-\nu}^* U_{l+1,\nu}^\dagger}{j\omega_0(\nu-p) - \mu_{l+1}^* - \mu_i} & \text{for } l > k-1 \end{cases} \quad (29)$$

### 2.3.3 The Reduced Single Oscillator Expressions.

The equivalent spectral densities for a single/free-running oscillator are found from the above expressions by substituting  $k = 1$ . The phase, amplitude and cross-correlation noise spectra defined above in eqs. (17), (25) and (27) are then reduced to the following single/free-running oscillator expressions

$$\mathfrak{L}^{(\nu)}(\omega_m^{(\nu)}) = \frac{\omega_0^2 \nu^2 c}{(0.5\omega_0^2 \nu^2 c)^2 + (\omega_m^{(\nu)})^2} \quad (30)$$

$$\mathcal{A}^{(\nu)}(\omega_m^{(\nu)}) = \sum_{\rho} \sum_{l=1}^{n-1} \frac{W_{l\rho}^{(\nu)} [2|\mu_{l+1,r}| + (\omega_0^2 \rho^2 c)] + 2T_{l\rho}^{(\nu)} [\omega_m^{(\nu)} + \mu_{l+1,i}]}{(|\mu_{l+1,r}| + (0.5\omega_0^2 \rho^2 c))^2 + (\omega_m^{(\nu)} + \mu_{l+1,i})^2} \quad (31)$$

$$\mathcal{R}^{(\nu)}(\omega_m^{(\nu)}) = -\frac{t^{(\nu)}(\omega_0^2 \nu^2 c) + 2u^{(\nu)}\omega_m}{(0.5\omega_0^2 \nu^2 c)^2 + (\omega_m^{(\nu)})^2} + \sum_{\rho} \sum_{l=1}^{n-1} \frac{E_{l\rho}^{(\nu)} [2|\mu_{l+1,r}| + (\omega_0^2 \rho^2 c)] + 2Z_{l\rho}^{(\nu)} [\omega_m^{(\nu)} + \mu_{l+1,i}]}{(|\mu_{l+1,r}| + (0.5\omega_0^2 \rho^2 c))^2 + (\omega_m^{(\nu)} + \mu_{l+1,i})^2} \quad (32)$$

where the various operators are defined above in sections 2.3.1 and 2.3.2 with  $k = 1$ . The results in eqs. (30) to (32) agree with the prior published results in [8–10]. Specifically, the reduced (single oscillator) PNOISE expression in eq. (30) represents simple Lorentzian functional characteristic of the offset frequency<sup>8</sup>, a well-established result [8, 9]. This outcome, once again, underscores the important fact, that the novel COSC-PMM framework not only extends the earlier published single oscillator PMM scheme but also entirely replaces it. A notable innovation, resulting from the COSC-PMM framework, has been the complete recalibration of how we approach time-domain macro-modelling of oscillator noise-response. It is now understood that the established PMM framework (see [8–10]), while representing an extremely impressive theoretical achievement, is indeed, without hyperbole, incomplete. The PMM represents a scope limited description which only covers a very minute subset of possible relevant circuits; namely the subset of free-running oscillators/clocks in the set of all oscillating circuits. The novel COSC-PMM methodology, on the other hand, is complete, and it replaces the old PMM description by extending the model domain to include the entire set of all possible oscillating autonomous networks.

## 2.4 Implementing the QUCS-COPEN PNOISE Module.

The QUCS-COPEN PNOISE module kernel algorithm is outlined in algorithm. 1. The module code is encapsulated within the new `pnsolver` C++ class which is part of the modified `qucsator` engine codebase (see [6] and footnote 2). The `pnsolver` C++ class inherits directly from the established `nasolver` class, which represent the base-class interface to all QUCS analysis classes. This new PNOISE module introduces a novel, previously absent, large-signal noise analysis utility to the `qucsator`/QUCS API.

Each instance of the `pnsolver` analysis class is given a reference to a single corresponding `pssolver` instance/object which is assumed to produce the large-signal PSS solution required to calculate the noise-response (see sections 2.1 and 2.2). The implementation of the `pssolver` object class was discussed in [6]. The `pssolver` reference object is identified through the string input parameter, `PssSim`, and the program fails to execute if no instance with this name exists in the schematic. The main routine, outlined in algorithm. 1, can be subdivided into three sub-procedures, referred to as `SubProc. I-III`.

### 2.4.1 SubProc. I : the Floquet Decomposition.

Starting on algorithm. 1 in algorithm. 1, this portion of the code is concerned with calculating the spectral Floquet operators  $\{U_{i,j}, \Lambda_{i,j}\}$ , introduced in section 2.2 and which are needed in-order to calculate the various noise operators in eqs. (17) to (19) and (25) to (29). In-order to achieve this goal the corresponding time-domain Floquet objects (see section 2.1),  $u_i(t)$ , and  $\lambda_i(t) = v_i^T(t)B(x_s(t))$  are first derived.

First, the (adjoint) monodromy matrix (MM) is evaluated through a call to `CalcMonodromy`, with the switch `ADJOINT` controlling whether the standard or adjoint MM is derived using the formulae in eq. (4) or eq. (8), respectively<sup>9</sup>. The (dual) Floquet vectors,  $\{u_{i0}, v_{i0}\}$ , and Floquet exponents,  $\{\mu_i\}$ , are then derived from the eigen-decomposition (note that  $\mu_i = \log(\lambda_i)/T_0$ , see section 2.1) of this (adjoint) MM using a standard QR Shur-shift algorithm routine, referred to in algorithm. 1 as `CalcEigenSet`.

Some of the calculated Floquet modes are dampened to an extent where they do not contribute noticeably to the spectral output at any offset above the noise-floor including the modes spanning the null-space of the (potentially) singular  $C$

<sup>8</sup>Consider the spectrum around the first harmonic,  $\nu = 1$ , with simplified notation  $\mathfrak{L}(\omega_m) \equiv \mathfrak{L}^{(1)}(\omega_m^{(1)})$ . From eq. (30),  $\mathfrak{L}(\omega_m) \approx (0.5\omega_0^2 c)/\omega_m^2$  for  $\omega_m \gg 0.5\omega_0^2 c$  which holds for most offsets of interest as  $c \ll 1$ . Thus, for most offset of interest,  $10 \log_{10}(\mathfrak{L}(\omega_m)) \approx 10 \log_{10}(0.5\omega_0^2 c) - 20 \log_{10}(\omega_m)$ , *i.e.* a straight line on a semi-log plot, which drops 20dB/decade.

<sup>9</sup>Note, that when integrating the (adjoint) LR equations in eqs. (2) and (6), for the purpose of deriving eqs. (4) and (8), the LR equations should be integrated using the same Linear-Multi-Step (LMS) setup as was used for calculating the PSS (see discussion in [6]). Also note that the adjoint equations must be integrated backwards in time [8, 16].

**Algorithm 1** QUCS-COPEN PNOISE Module Kernel.

---

**Parameters :** Start, Stop, Type, N ▷ freq. swp range, type [lin/log] & # points/(dec)  
**Parameters :** Nf, NoiseNodes, ▷ Nf : # harmonics, NoiseNodes : output node-names.  
**Parameters :** k, PssSim ▷ k : # osc. units, PssSim : PSS ref. obj. name.  
**Input :**  $x_{PSS}(t)$  ▷ calculated PSS solution.  
**Output Datasets :** pnoise (Xpn), xcorr (Xcr), anoise (Xan) ▷ DS file ext. with X=[V/I], Volt./Current.  
**Require:** Start > 0, Stop > Start, N(Type=lin|log) ≥ 10|3, Nf ≥ 16  
**Ensure:** isNodeArray(noiseNodes) = true ▷ check : all input nodes exist in circ.  
**Ensure:** isNum( $x_{PSS}$ ) and isPeriodic( $x_{PSS}$ ) = true ▷ check :  $x_{PSS}$  is valid PSS solution.  
**Ensure:** moduleExists(PssSim) = true ▷ check : reference PSS module exist in schematic.

---

1: SubProc. I : Calculate Floquet Decomposition.

---

2:  $\Phi_{MM} \leftarrow \text{CalcMonodromy}(T_0; x_{PSS}, \text{ADJOINT=false})$  ▷ calc. standard monodromy from eq. (4).  
3:  $\Psi_{MM} \leftarrow \text{CalcMonodromy}(T_0; x_{PSS}, \text{ADJOINT=true})$  ▷ calc. adjoint monodromy from eq. (8).  
4:  $\{u_{i0}, \mu_i\}_{i=1}^n \leftarrow \text{CalcEigenSet}(\Phi_{MM})$   
5:  $\{v_{i0}, \mu_i\}_{i=1}^n \leftarrow \text{CalcEigenSet}(\Psi_{MM})$   
6:  $B(t) \leftarrow \text{NoiseMatrixSeries}(x_{PSS})$   
7:  $L \leftarrow \text{NumberRelevantModes}(\{\mu_i\}, T_0)$  ▷ count # relevant Floquet modes.  
8: **for**  $j = 1 \rightarrow L$  **do**  
9:  $u_j(t) \leftarrow \text{LrIntegrate}(u_{j0}, \text{ADJOINT=false})$  ▷ integrate eq. (2) **fwd** in time with init. cond.  $u_{j0}$ .  
10:  $v_j(t) \leftarrow \text{LrIntegrate}(v_{j0}, \text{ADJOINT=true})$  ▷ integrate eq. (6) **bwd** in time with init. cond.  $v_{j0}$ .  
11:  $\lambda_j(t) \leftarrow \text{generateLambda}(B(t), v_j(t))$  ▷ calculate :  $\lambda_j(t) = v_j^\top(t)B(t)$   
12:  $U_j \leftarrow \text{VectorFFT}(u_j(t), \text{Nf})$   
13:  $\Lambda_j \leftarrow \text{VectorFFT}(\lambda_j(t), \text{Nf})$   
14: **end for**

---

15: SubProc. II : Calculate Noise Operators.

---

16:  $c \leftarrow \text{CalcPhaseDiff}(\Lambda_1)$  ▷ calc. phase diff. const., see section 2.1.2.  
17: **params**  $\leftarrow \text{struct}(k, \nu, c, T_0, \text{Nf}, L, \{U_i, \mu_i, \Lambda_i\})$   
18: **for** ndName in noiseNodes **do**  
19:  $q \leftarrow \text{NodeName2Index}(\text{ndName})$  ▷  $q$  : state vec. index corresp. to ndName.  
20:  ${}_q\Omega^{(\nu)} \leftarrow \text{CalcOmegaMatrix}(q, \text{params})$  ▷ eval.  $q$ th diagonal comp. of eq. (18)  
21:  ${}_q\Upsilon^{(\nu)} \leftarrow \text{CalcUpsilonMatrix}(q, \text{params})$  ▷ eval.  $q$ th diagonal comp. of eq. (28)  
22: **for**  $\rho = -\text{Nf} \rightarrow \text{Nf}$  **do**  
23: **for**  $l = 1 \rightarrow k - 1$  **do**  
24:  ${}_q\Theta_{l\rho}^{(\nu)} \leftarrow \text{CalcThetaTensor}(l, \rho, q, \text{params})$  ▷ eq. (19) @ index  $(l, \rho)$ , ( $q$ th diag. comp.).  
25: **end for**  
26: **for**  $l = 1 \rightarrow L - k$  **do**  
27:  ${}_q\Pi_{l\rho}^{(\nu)} \leftarrow \text{CalcPiTensor}(l, \rho, q, \text{params})$  ▷ eq. (26) @ index  $(l, \rho)$ , ( $q$ th diag. comp.).  
28: **end for**  
29: **for**  $l = 1 \rightarrow L$  **do**  
30:  ${}_q\Xi_{l\rho}^{(\nu)} \leftarrow \text{CalcXiTensor}(l, \rho, q, \text{params})$  ▷ eq. (29) @ index  $(l, \rho)$ , ( $q$ th diag. comp.).  
31: **end for**  
32: **end for**  
33: **end for**

---

34: SubProc. III : Calculate Noise Spectra & Save Datasets.

---

35: **Fsweep**  $\leftarrow \text{GenerateSweep}(\text{Start}, \text{Stop}, \text{Type}, \text{N})$   
36: **params**  $\leftarrow \text{struct}(k, \nu, T_0, \text{Nf})$   
37: **for** ndName in noiseNodes **do**  
38:  $q \leftarrow \text{NodeName2Index}(\text{ndName})$   
39:  $i \leftarrow 0$   
40: **for** fm in **Fsweep** **do**  
41:  $\text{pnoise}[i] \leftarrow \text{calcPnoise}(q, \text{fm}, \text{params}, \Omega^{(\nu)}, \Theta_{l\rho}^{(\nu)})$  ▷ eval. phase noise spectrum, see eq. (17)  
42:  $\text{anoise}[i] \leftarrow \text{calcAnoise}(q, \text{fm}, \text{params}, \Pi_{l\rho}^{(\nu)})$  ▷ eval. amp. noise spectrum, see eq. (25)  
43:  $\text{xnoise}[i] \leftarrow \text{calcXnoise}(q, \text{fm}, \text{params}, \Upsilon^{(\nu)}, \Xi_{l\rho}^{(\nu)})$  ▷ eval. xcorr noise spectrum, see eq. (27)  
44:  $i \leftarrow i + 1$   
45: **end for**  
46: **SaveDatasets**(ndName, **Fsweep**, pnoise, anoise, xnoise) ▷ Store ndName datasets for print.  
47: **end for**

---

Jacobian matrix (see eqs. (1) and (2)), which corresponds to modes with negative infinite Floquet exponents (real part),  $\lambda_i = 0 \Rightarrow \Re\{\mu_i\} = -\infty$ . Since these types of modes do not contribute to the visible part of the calculated spectrum (above the noise floor) it is only natural to neglect these contributions. Doing so will shrink the size of the effective Floquet set and thus significantly improve the computational efficiency of the algorithm. From [18], the so-called, *relevant modes*, satisfy  $|\Re\{\mu_i\}| \ll \omega_0$  and for our purposes this translates into the rule  $\Re\{\mu_i\} \leq 10\omega_0$ . On algorithm. 1 of algorithm. 1 the call to `NumberRelevantModes` counts these modes, according to the mentioned rule, thus allowing us to shrink the effective Floquet set to from  $n$  to  $L \leq n$  modes. Next, the noise-matrix,  $B(x_s(t))$ , defined in eq. (1), is then evaluated by probing the circuit noise source contributions along the PSS,  $x_s(t)$ . This is done in algorithm. 1 with a call to `NoiseMatrixSeries`.

The time-series of the  $j$ th (dual) Floquet vector  $u_j(t), v_j(t)$  is derived by integrating the (adjoint) LR equations in eq. (2) and eq. (6), respectively with initial conditions,  $\{u_{j0}, v_{j0}\}$ , (backwards) forwards in time. These calculations are done with a call to `LRintegrate` with the switch `ADJOINT` controlling whether the standard LR equations in eq. (2) or the adjoint version in eq. (5) are invoked. Finally, the lambda-operators can be formed (`generateLambda` on algorithm. 1) and the corresponding spectral operators, mentioned above, are evaluated by a call to a standard FFT library routine.

## 2.4.2 SubProc. II + III : Calculate Noise Operators & Output Spectra.

The second part of algorithm. 1 starts on algorithm. 1. It concerns the calculation of the noise operators defined in sections 2.2 and 2.3. Expressions such as *e.g.* eqs. (18), (19) and (26) *etc.*, all involve infinite sums, represented in the equations as summations without limits. An example hereof could be the summation,  $\sum_p$ , in eq. (28), with  $p \in ]-\infty; \infty[$ . The index variables, referenced in these infinite sums, all label harmonics of Fourier transformed operators. Hence, as written in *e.g.* eqs. (18), (19) and (26), these expressions all assume infinite harmonic contributions. Obviously, for the algorithm considered here, the range of these sums must be capped. Thus, in algorithm. 1, all harmonic sums are restricted to the domain,  $[-Nf, Nf]$ , where `Nf` is an input parameter (see parameter section of algorithm. 1).

The main procedure involves several nested for loops with the outermost loop iterating over the set of observation/measurement nodes provided by the input parameter string-list `NoiseNodes`. From the discussion in section 2.2, and in [7], the aim of the algorithm should be to calculate the auto-correlation spectrum of a given measurement node. Hence, for a measurement index,  $q$ , corresponding to a circuit node name in `NoiseNodes`, only the  $q$ th diagonal element of the noise-correlation spectrum needs to be calculated. This, in-turn, implies that only  $q$ th diagonal element of the various noise operators, discussed here and in section 2.2, must be calculated. For the matrices  $\Omega^{(\nu)}$  and  $\Psi^{(\nu)}$ , defined in eqs. (18) and (28), this element is written  ${}_q\Omega^{(\nu)}, {}_q\Psi^{(\nu)}$  with the notation explained in footnote 7. Similarly, the 3 tensors  $\Theta_{l\rho}^{(\nu)}, \Pi_{l\rho}^{(\nu)}, \Xi_{l\rho}^{(\nu)}$ , defined in eqs. (19), (26) and (29) are calculated for indices,  $l, \rho$ , where harmonic index  $\rho$  runs from  $-Nf$  to  $Nf$  and the domain of index,  $l$ , depends on the specific operator being calculated.

The last portion of the QUCS-COPEN PNOISE algorithm in algorithm. 1 start on algorithm. 1 and involves calculating the various COSC-PMM spectra defined in eqs. (17), (25) and (27). To do so, the procedure employs the various noise-operators calculated in Proc. II. The spectra are calculated for each node in the array `NoiseNodes` and then stored to datasets, which are then printed according to internal `qucsator` procedures.

## 2.5 The GUI Environment & Output Datasets.

Various details and issues *w.r.t.* the QUCS-COPEN GUI was discussed in [6]. Figure 1 displays the newly implemented PNOISE tool operating inside the QUCS-COPEN GUI application (QUCS-S clone, see footnote 2) along with the required companion PSS module, which is referenced by the PNOISE input string parameter `PssSim` (see algorithm. 1). The figure shows the result of running a PSS+PNOISE simulation for some unspecified oscillator circuit. The PNOISE simulator outputs 3 datasets (DS) referenced by the corresponding file extensions : the phase-noise spectrum  $\{.Vpn, .Ipn\}$ , the amplitude noise spectrum  $\{.Van, .Ian\}$ , and the phase-amplitude cross-correlation noise spectrum (not shown)  $\{.Vxn, .Ixn\}$ .

## 3 Example Oscillator Circuits.

Below, the QUCS-COPEN PNOISE module, plus the mandatory companion PSS solver, are applied to three different single/free-running oscillator circuits. Then, in section 3.2, a coupled oscillator network is considered. As far as the authors can tell, the tool demonstrated here, performing noise-response analysis of large-signal nonlinear (coupled) oscillating circuits, represents the first successful implementation of its kind into the QUCS ecosystem. All the circuits

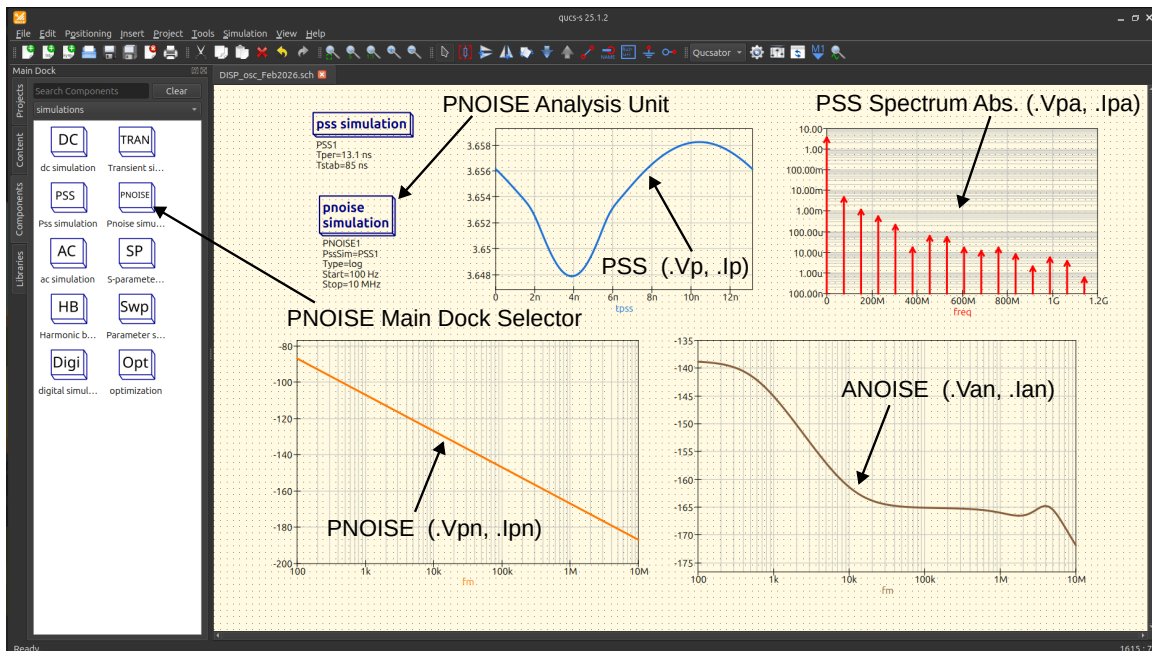


Figure 1: The figure shows the QUCS-COPEN PSS+PNOISE simulation units integrated into the QUCS-S GUI environment. Both the PNOISE and PSS reference modules are chosen from the main-dock and then placed on the schematic. The PNOISE & PSS modules are linked through the PNOISE parameter `PssSim` (see algorithm. 1). PSS & PNOISE datasets (unspecified circuit & output node), with file extensions, **blue graph** : PSS time-domain solution, (.Vp, .Ip), **red graph** : PSS spectrum, absolute value, (.Vpa, .Ipa), which is plotted in dBm, **orange graph** : Phase noise spectrum, in dBc, (.Vpn, .Ipn) and **brown graph** : Amplitude noise spectrum, in dBc (.Van, .Ian).

considered here, with just a few minor modifications (*e.g* addition of external noise sources), were also discussed in [6] in the context of the QUCS-COPEN PSS module (steady-state analysis). For this reason, only very brief descriptions of these circuits will be given below. For further details, please refer to [6, sec. 3].

The first oscillator circuit, shown fig. 2 and known throughout as OSC.#1, is a simple Van-der-Pol equivalent configuration, first proposed in [7]. The PSS module calculates a solution with oscillation frequency  $f_0 = 1/T_0 = 896.6\text{MHz}$  and the figure plots the relevant PSS & PNOISE datasets (see fig. 1 caption). Figure 3 displays the same simulation setup as in fig. 2, but this time for a BJT Collpitts oscillator first proposed in the paper [9]. Below this circuit is referred to as OSC.#2. Compared with the original oscillator design in [9], the circuit in fig. 3 includes a few modifications (see [6] for details). Finally, fig. 4 shows the PNOISE module applied to a MOSFET cross-coupled pair, LC tank oscillator, referred to herein as OSC.#3. The circuit is similar to the MOSFET oscillator proposed in [18, fig. 3] including identical device models with a few slight modifications (see [6] for details). The PSS simulator finds a solution oscillating at,  $f_0 = 888.6\text{MHz}$ , and the PSS+PNOISE output datasets, introduced in fig. 1, are plotted.

### 3.1 Coupled Oscillator Example Circuit.

As mentioned in sections 2.2 and 2.3.3, the COSC-PMM methodology, introduced in [7], both extends and replaces the earlier single-oscillator PMM framework, developed in [8–10]. The replacement claim was directly proven in section 2.3.3 and further investigated in the free-running oscillator examples discussed above. The new model extends the earlier framework by expanding the scope to include all oscillating configurations, including coupled systems. In this section the QUCS-COPEN PNOISE module is applied to a coupled circuit; an injection-locked oscillator (ILO) configuration, referred to here COSC.#1.

The schematic of the COSC.#1 ILO circuit is displayed in fig. 5. It consists of two oscillator units, included in the schematic as sub-circuit components, of OSC.#1-type<sup>10</sup> (see fig. 2), coupled through a unilateral buffer amplifier. The *primary oscillator*, PRM-OSC, injects its output signal, through the unilateral buffer amplifier, into the *secondary*

<sup>10</sup>Let CIR.#A represent some circuit. Then we say that that CIR.#B is of CIR.#A-type<sup>10</sup> if CIR.#B has the same topology (*i.e.* same set of components & connections), but possibly, different component values. .

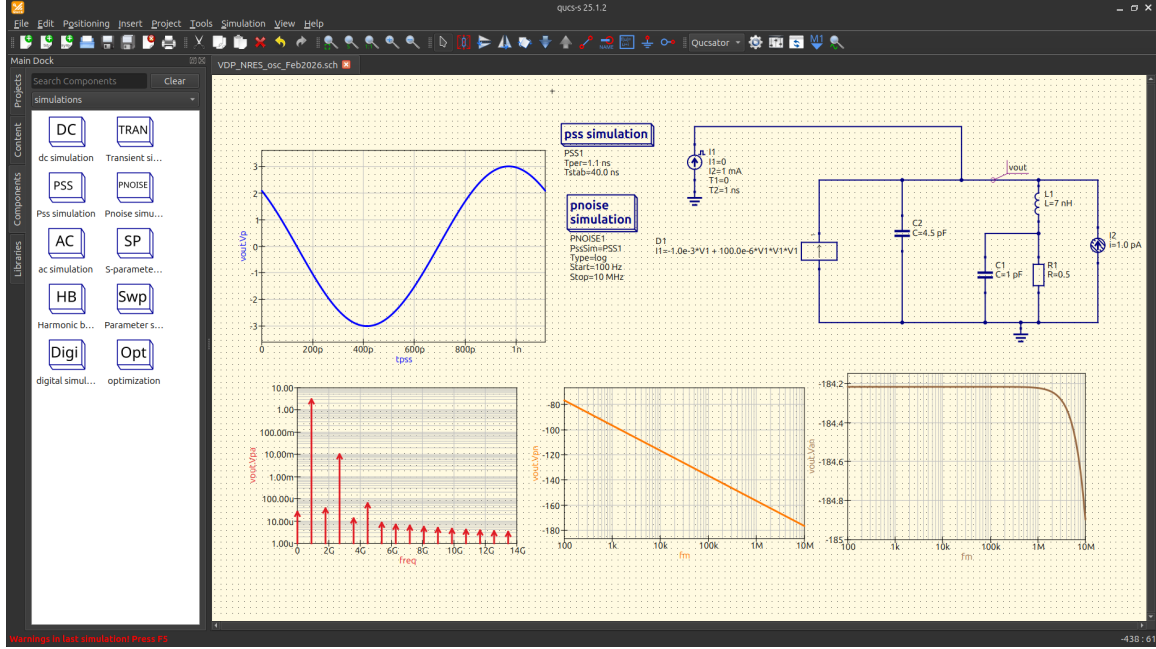


Figure 2: The QUCS-COPEN PNOISE calculator module applied to a simple Van-der-Pol(VDP)-type oscillator, proposed in [7, Fig. 3]. This circuit is referred to below as OSC.#1. All parameters (including the external noise source) are as in [7, Fig. 3] (primary osc. parameter set). The datasets introduced in fig. 1 are plotted for the voltage node, vout. Refer to fig. 1 caption for further details.

oscillator, SEC-OSC. The circuit parameters of the two oscillator units are chosen as the primary/secondary values listed in [7, figure 3 caption]. The coupling buffer is linear with trans-conductance  $g_m = 50.0 \mu\text{S}$ . The circuit in fig. 5 represents a 2-ensemble (see section 2.2), as it is constructed by coupling 2 independent free-running oscillator units which implies  $k = 2$ . Here, the COSC-PMM model parameter,  $k$ , represents the number of oscillator units in the coupled ensemble (see sections 2.2 and 2.3 and algorithm. 1).

Figure 5, plots the various relevant datasets corresponding to output nodes of both oscillators in the schematic. Considering the PNOISE spectra (orange graphs), the PRM-OSC graph (dashed line) is seen to follow the standard free-running Lorentzian characteristic (see figs. 2 to 4 and footnote 8). This makes sense as, from the above description, the PRM-OSC circuit must be free-running. In contrast, assuming synchronization is achieved, the SEC-OSC oscillator circuit must be phase-locked, and hence also frequency-locked, to the PRM-OSC source. From established ILO noise-response theory (see e.g. [19, 20]) this implies a non-Lorentzian PNOISE spectral characteristic and inspecting the corresponding spectral graph in fig. 5 (orange solid line) this is indeed the case. The QUCS-COPEN PNOISE module, implemented herein, applies the rigorous COSC-PMM methodology and is hence able to correctly (*i.e.* without using any empirical/phenomenological modelling tools) capture the noise-response of both free-running and coupled circuits. The open-source QUCS-COPEN simulator project is the first ever, to our knowledge at-least, EDA program, either open-source or commercial, to come equipped with a noise analysis tool of this caliber.

### 3.2 Verification of the Obtained PSS Solutions & Convergence Tests.

Define the measure,  $\Delta_{\mathcal{L}} = (\mathcal{L}^{\text{QC}}(1\text{kHz}) - \mathcal{L}^{\text{K-ADS}}(1\text{kHz}))/\mathcal{L}^{\text{QC}}(1\text{kHz})$ . Here,  $\mathcal{L}^{\text{QC}}(f_m)$  and  $\mathcal{L}^{\text{K-ADS}}(f_m)$  are the phase-noise spectra, at offset frequency  $f_m$  in a 1 Hz bandwidth measured in dBc (see discussion in section 3) and evaluated using the novel QUCS-COPEN PNOISE tool (QC) and the commercial Keysight-ADS<sup>®</sup> pnm simulator (K-ADS), respectively. Thus,  $\Delta_{\mathcal{L}}$  records, for a given oscillator circuit, the relative deviation of phase-noise measurements evaluated @  $f_m = 1\text{kHz}$ , produced using these two very different EDA programs. This type of discrete frequency verification scheme is valid when considering free-running oscillators due the special form of the PNOISE spectra produced by these circuits (see eq. (30), footnote 8, and figs. 2 to 4). Table 1 displays the calculated phase-noise values and the resulting absolute measure,  $|\Delta_{\mathcal{L}}|$ , for each of the three oscillators discussed above in section 3. The maximum recorded error is  $|\Delta_{\mathcal{L}}| \sim 0.03\%$ , or  $|\Delta_{\mathcal{L}}| \sim 300\text{ppm}$  (parts-per-million). The results listed in table 1 serve to validate the developed QUCS-COPEN PNOISE tool.

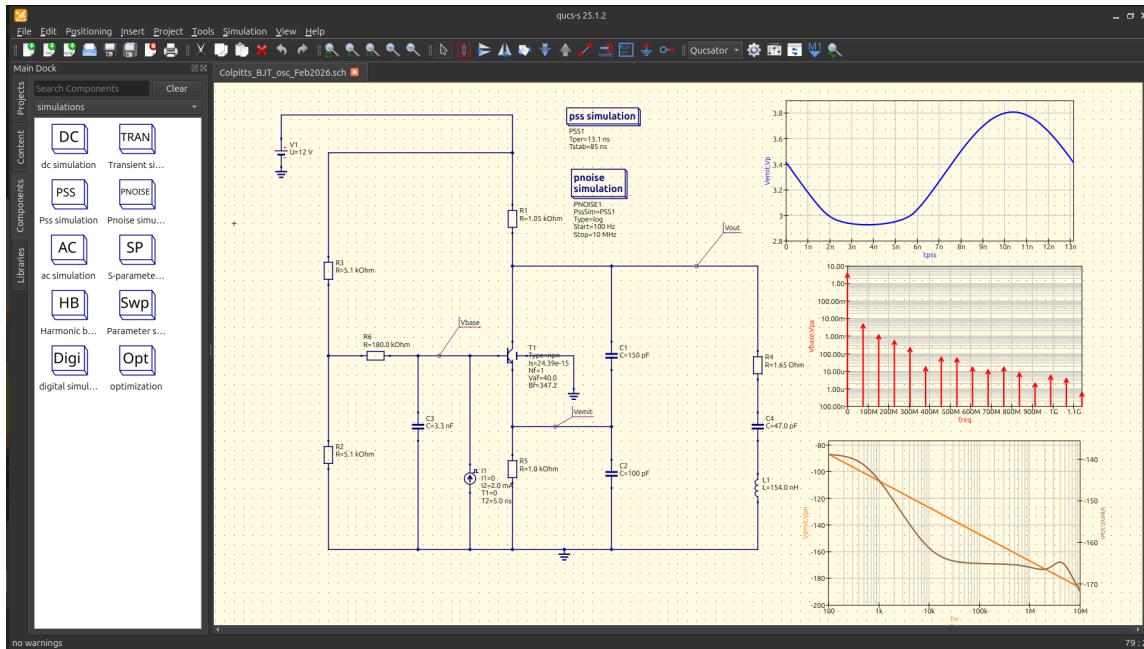


Figure 3: The QUCS-COPEN PNOISE module is applied to a BJT Colpitts oscillator taken from [9], referred to below as OSC.#2. All circuit parameters as in [9], with a few minor exceptions (see [6] for details). In this simulation the BJT device is noiseless except for internal resistor contributions. The PSS+PNOISE datasets, introduced in fig. 1, are plotted for the BJT emitter node (called  $V_{emitt}$  in schematic). See fig. 1 for further details.

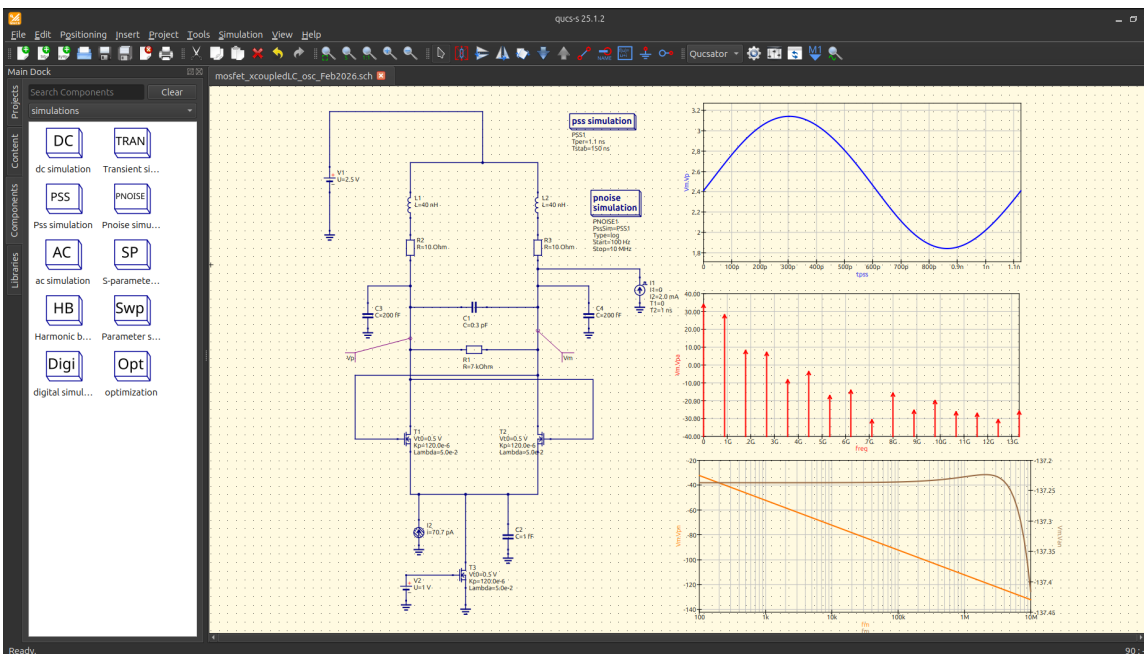


Figure 4: The QUCS-COPEN PNOISE simulation tool applied to a MOSFET cross-coupled LC-tank oscillator, referred to below as OSC.#3, similar to the oscillator proposed in [18, fig. 3] with minor modifications(see [6] for details). All parameters (including the external noise source) are as in [7, Fig. 3]. The PSS & PNOISE datasets, introduced in fig. 1, are plotted for the right MOSFET right drain node  $V_m$ . See also fig. 1 for further details.

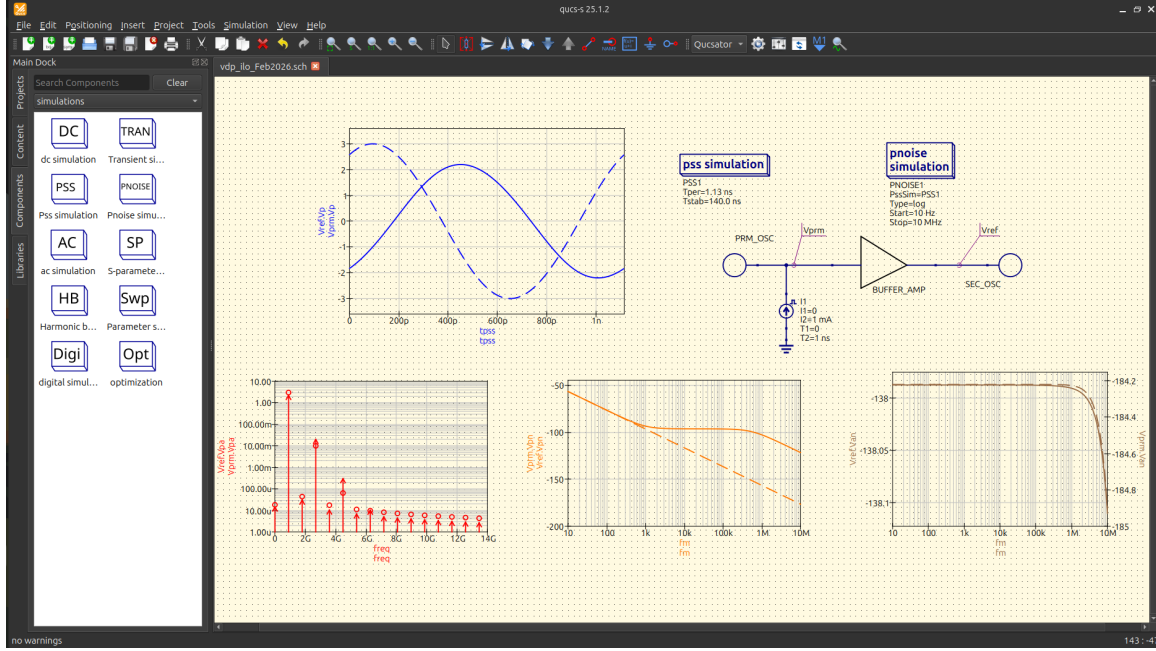


Figure 5: The QUCS-COPEN PNOISE module is applied to an injection-locked circuit (ILO) configuration referred to as COSC.#1 (see text for details). Relevant datasets (see fig. 1) are plotted for the output nodes of both the primary (dashed line plots) and secondary (solid line plots) oscillator nodes. In the schematic these nodes are referred to as  $V_{prm}$  and  $V_{ref}$ , respectively. It is immediately observed that the calculated secondary oscillator ( $V_{ref}$ ) PNOISE spectrum (orange solid line plot) does not follow the standard Lorentzian profile (see footnote 8).

	QUCS-COPEN	Keysight-ADS <sup>©</sup>	$ \Delta_{\mathcal{L}} $
OSC.#1	-96.62355963dBc	-96.62509613dBc	0.00159%
OSC.#2	-106.8649804dBc	-106.8350436dBc	0.02801%
OSC.#3	-52.20484281dBc	-52.21153470dBc	0.01281%

Table 1: The table lists oscillator PNOISE spectra (around 1st harmonic), evaluated @  $f_m = 1\text{kHz}$ , calculated using the QUCS-COPEN package and the commercial Keysight-ADS<sup>©</sup> simulator for circuits : OSC.#1 = VDP circuit in fig. 2, OSC.#2 = BJT circuit in fig. 3 and OSC.#3 = MOSFET circuit in fig. 4. The relative deviation between the calculated values are recorded by measure  $\Delta_{\mathcal{L}}$  (see text in section 3.2).

Figure 6 plots the PNOISE spectrum of two coupled oscillator configurations (COSC.#2 & COSC.#3), calculated using the QUCS-COPEN PNOISE module and the Keysight-ADS<sup>©</sup> pnm algorithm, for 3 sets of coupling parameters denoted C-SET #1-3. The block diagrams describing the coupling topology of these two circuits are shown in fig. 6.(a). Here, COSC.#2 includes 3 independent oscillator units (3-ensemble), of OSC.#1-type (see footnote 10), coupled bilaterally through resistive coupling. The specific component values chosen for this circuit are reported in [7, Fig. 7]. The second circuit in fig. 6.(a) is an ILO, similar to COSC.#1 considered in fig. 5, but with the secondary oscillator represented by a OSC.#3-type circuit (see footnote 10 and fig. 4). Then in fig. 6.(b) the PNOISE spectra these two coupled circuits are plotted for each of the parameter (coupling) sets C-SET #1-3, which are identical to the 3 parameter sets reported in [7, Table 1]. Inspecting fig. 6.(b), the calculated solution follows the reference produced by the commercial Keysight-ADS<sup>©</sup> pnm algorithm for all offsets considered.

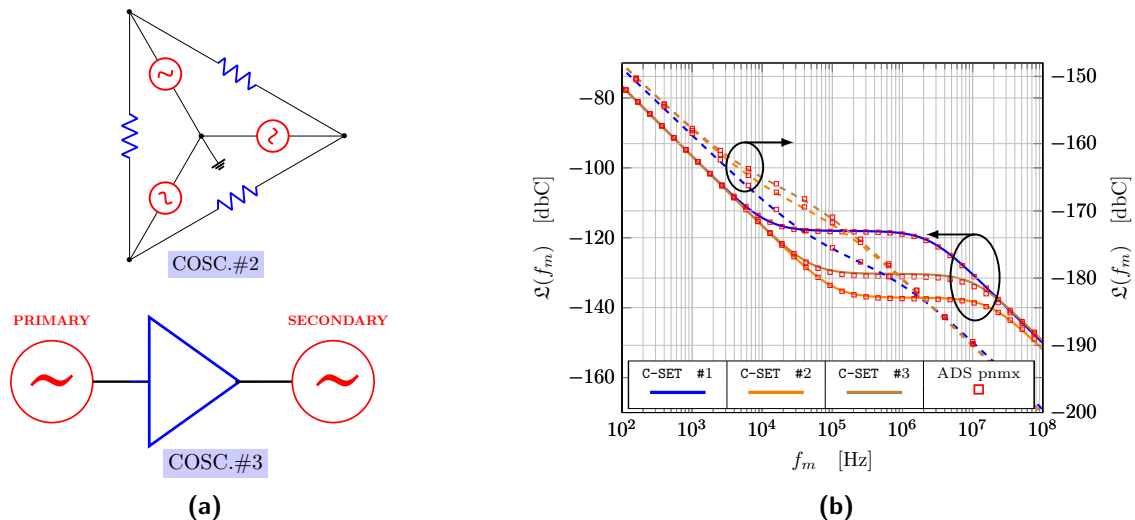


Figure 6: PNOISE spectra of coupled oscillator circuits calculated using the QUCS-COPEN PNOISE module and with the commercial Keysight-ADS<sup>®</sup> pnmix routine employed as a reference. (a) : the two coupled circuits considered here are COSC.#2 & COSC.#3 (see text for details). (b) : The PNOISE spectra are calculated for each of the coupled circuits in (a) with COSC.#2 (leftmost osc. node) drawn with **dashed line** & COSC.#3 (secondary osc. node) drawn with **solid line**. The spectra are calculated for 3 levels of coupling strength, as specified by the parameter sets C-SET #1-3 (see text for details) with the graph color codes shown in the figure.

#### 4 Conclusion & Future Work.

The paper documents the development of a novel simulator analysis module aimed at calculating the response of noise-perturbed autonomous oscillating systems. The underlying algorithm is based on a state-of-the-art model proposed recently by the authors, and the solution was integrated into the newly established QUCS-COPEN EDA program; a clone of the open-source QUCS and QUCS-S projects. The developed QUCS-COPEN noise module is unique, employing a novel, unified and rigorous time-domain methodology to construct a robust and efficient algorithm uncorrupted by any phenomenological or empirical modelling techniques, and applicable to both free-running and coupled oscillating systems. Such features distinguish the implemented simulator from all other open-source and commercial EDA packages currently available, wherein noise analysis is, almost exclusively, performed by algorithms developed using some type of LTI or LTV theoretic approach, such as *e.g.* a conversion-matrix method. The proposed QUCS-COPEN simulator project materially advances the state-of-the-art as it concerns the field of EDA noise simulation, analysis, synthesis and optimization of coupled and free-running oscillating circuits. This class of circuits is ubiquitous in modern communication and remote-sensing systems and the robust and efficient numerical tools, developed herein, will turn out to have significant impact in various areas of industrial circuit design. The implemented solution was validated through a comparison-study with the commercial Keysight-ADS<sup>®</sup> EDA simulator program. Future work will focus on improving the robustness and efficiency of the implemented QUCS-COPEN simulation tools.

#### Acknowledgment

The authors gratefully acknowledge partial financial support by German Research Foundation (DFG) (grant no. KR1016/17-1).

#### References

- [1] S. Jahn, M. Margraf, V. Habchi, and R. Jacob. Qucs technical papers. Technical report, 2007.
- [2] S. Jahn and J. C. Borrás. Getting started with qucs. Technical report, March 2007.
- [3] Mike Brinson and Vadim Kuznetsov. Qucs equation-defined and verilog-a rf device models for harmonic balance circuit simulation. In *2015 22nd International Conference Mixed Design of Integrated Circuits & Systems (MIXDES)*, pages 192–197. IEEE, 2015.

- [4] Mike Brinson and Vadim Kuznetsov. Qucs-0.0. 19s: A new open-source circuit simulator and its application for hardware design. In *2016 International Siberian Conference on Control and Communications (SIBCON)*, pages 1–5. IEEE, 2016.
- [5] Mike Brinson and Vadim Kuznetsov. Improvements in qucs-s equation-defined modelling of semiconductor devices and ic's. In *2017 MIXDES-24th International Conference" Mixed Design of Integrated Circuits and Systems*, pages 137–142. IEEE, 2017.
- [6] Torsten Djurhuus and Viktor Krozer. A novel phase-noise module for the qucs circuit simulator. part i: the periodic steady-state. *arXiv preprint arXiv:2512.10373*, 2025.
- [7] Torsten Djurhuus and Viktor Krozer. A generalized model of coupled oscillator phase-noise response. *International journal of circuit theory and applications*, 50(1):35–55, 2022.
- [8] A. Demir, A. Mehrotra, and J. Roychowdhury. Phase noise in oscillators: a unifying theory and numerical methods for characterization. *IEEE Transactions on Circuits and Systems I: Fundamental Theory and Applications*, 47(5):655–674, 2000.
- [9] Franz X Kaertner. Analysis of white and f-  $\alpha$  noise in oscillators. *International Journal of Circuit Theory and Applications*, 18(5):485–519, 1990.
- [10] Fabio L Traversa and Fabrizio Bonani. Oscillator noise: A nonlinear perturbative theory including orbital fluctuations and phase-orbital correlation. *IEEE Transactions on Circuits and Systems I: Regular Papers*, 58(10):2485–2497, 2011.
- [11] Almudena Suarez. *Analysis and design of autonomous microwave circuits*. John Wiley & Sons, 2009.
- [12] GNU Project - the Free Software Foundation. *GnuCap Manual*, January 2024. Available at <http://www.gnucap.org/dokuwiki/doku.php/gnucap:manual:introduction>.
- [13] Paolo Nenzi Holger Vogt, Giles Atkinson. *Ngspice User's Manual Version 44plus*, June 2025. Available at <https://ngspice.sourceforge.io/docs/ngspice-manual.pdf>.
- [14] Eric R. Keiter. *Xyce™ Parallel Electronic Simulator User's Guide*. Sandia National Lab.(SNL-NM), Albuquerque, NM (United States), 2025. Available at <https://xyce.sandia.gov/documentation-tutorials/>.
- [15] Bjarne Stroustrup. *The C++ programming language*. Pearson Education, 2013.
- [16] Alper Demir. Phase noise in oscillators: Daes and colored noise sources. In *Proceedings of the 1998 IEEE/ACM international conference on Computer-aided design*, pages 170–177, 1998.
- [17] Torsten Djurhuus, Viktor Krozer, Jens Vidkjær, and Tom K Johansen. Oscillator phase noise: A geometrical approach. *IEEE Transactions on Circuits and Systems I: Regular Papers*, 56(7):1373–1382, 2008.
- [18] Paolo Maffezzoni, Federico Pepe, and Andrea Bonfanti. A unified method for the analysis of phase and amplitude noise in electrical oscillators. *IEEE transactions on microwave theory and techniques*, 61(9):3277–3284, 2013.
- [19] K Kurokawa. Some basic characteristics of broadband negative resistance oscillator circuits. *Bell System Technical Journal*, 48(6):1937–1955, 1969.
- [20] Torsten Djurhuus and Viktor Krozer. A novel first-principles model of injection-locked oscillator phase noise. *arXiv preprint arXiv:2501.02675*, 2025.